ISSN 2347-3487
Volume 13 Number 6
Journal of Advances in Physics

Hydrogen production using Al-Sn alloys prepared by rapid solidification

Y.M.Abbas[(1)], A. Hassan Ibrahim[(1)], S. Mosaad[(1)], M.Orabi[(1)]
[(1)] Physics Department, Faculty of Science, Suez Canal University, Egypt
ymabbas@gmail.com
[(1)] Physics Department, Faculty of Science, Suez Canal University, Egypt
Ahmedphysics.ah@gmail.com
[(1)] Physics Department, Faculty of Science, Suez Canal University, Egypt
saramosaad@windowslive.com
[(1)] Physics Department, Faculty of Science, Suez Canal University, Egypt
Ahmed_Abdel-Hamid@science.suez.edu.eg

Abstract

Air pollution produced by the direct burning of fossil fuels is a serious problem. Therefore, there is a vital demand for renewable and clean fuel replacements for future energy source. Hydrogen, which exhibits high calorific value and is a clean burning product, could be the first choice in the future, as it is a good-looking fuel for fuel cells where the electric energy is directly gotten by the electrochemical reactions of hydrogen and oxygen. Rapidly solidified Al_{100-x}-Sn_x alloy X= (0, 25, 55, 75 all in wt.%) was prepared using melt spinning technique at 800 °C. The structural and microstructural evolutions of the phases have been studied using X-ray powder diffraction (XRD) and the Rietveld method. $Al_{45}Sn_{55}$ alloy shows the best volume of hydrogen generation which is (531 ml), this alloy has the highest number of grains (1096) than other prepared alloys in its surface which examined through a Scanning electron microscope (SEM) and analyzed using an SPM data visualization and analysis tool (Gwyddion 2.32). Differential thermal analysis (DTA) was used for calculating melting temperature for all prepared alloys. Melting temperature reduced from 933.47 K for Al pure to 500.95 K in $Al_{45}Sn_{55}$ alloy. Temperature dependence of resistivity had been performed for all prepared alloys. Electrical properties of prepared alloys show the decrease in volume of the unit cell V with increasing VEC, which means that the volume of the first Brillouin zone increases by increasing VEC since they are inversely proportional to each other.

Keywords

Al-Sn alloy; Hydrogen generation; X-Ray Diffraction Analysis (XRD); Electrical Resistivity; Thermal analysis, Scanning electron microscope (SEM).

Academic Discipline And Sub-Disciplines

Physics; material science

SUBJECT CLASSIFICATION

Hydrogen generation

TYPE (METHOD/APPROACH)

Experimental

1. Introduction

The direct combustion of fossil fuels that produced air pollution is a dangerous environmental problem. Consequently, there is an urgent request for renewable and clean fuel alternatives for future energy source. Hydrogen, which displays high calorific value and clean combustion product, might be the first choice in the future, as it is a smart fuel for fuel cells where the electric energy is obtained directly by the electrochemical reactions of hydrogen and oxygen [1]. Furthermore, hydrogen has many wonderful advantages such as high energy density, non-polluted reaction products, and rich natural sources. Alternatively, hydrogen does not typically exist by itself in nature and must be generated from a number of compounds through a chemical reaction. Numerous methods can be used for hydrogen generation, such as the decomposition of fossil fuels, water splitting and a reaction of metals or alloys with water. Among the methods, especially, the technology based on the reaction of reactive metals with water to produce hydrogen has been explored broadly [2-4]. As an advanced application of a conventional technology, hydrogen production by corrosion of alloys and hydrolysis has been extensively studied [5]. In a metal reactions, Large amounts of hydrogen release occurs instantly after the metal is immersed, even in mild aqueous solutions. So, the reactions of metal allow a real-time hydrogen generation from aqueous mediums. A number of studies have surveyed the use of metals, including Zn, Al, and Mg, to produce hydrogen from aqueous solutions [6-12]. Amid the candidates, aluminum (Al) has been recognized as the most talented metal for hydrogen generation [13] because it is cheap and environmentally recyclable, produces hydrogen without carbon oxides, and provides a high hydrogen yield of up to 11.1 wt%. On the other hand, the inactive film can form easily on the Al surface during the hydrogen generation, which decreases the hydrogen production rate. Numerous methods such as the use of chemical additives in solutions and the addition of alloying elements in Al alloys have been considered to stop the creation of inactive film and accelerate the corrosion of the alloy surface. Especially, the hydrogen generation rate has been reported to be increased by the addition of elements such as Fe, Ni and Cu, owing to the precipitation of phases like Al_2Cu, Al_3Fe, and Al_3Ni along the grain boundary of aluminum [14-16]. Moreover, Al-Si alloys were reported to have the

highest initial H_2 generation in alkaline water. It has also been reported that hydrogen can be produced by the reaction of Si with an alkaline solution of NaOH [17]. However, another metal is needed to activate the reaction between Si and water to produce H_2, due to the low activity of Si, and Al can be used for this persistence [18]. Tin (Sn) was chosen for preparing the Al alloy. Al-Sn alloy reactants were investigated by changing the alloy content and microstructure.

2. Characterization Techniques

The phase identification and crystal structure of the rapidly solidified Al-Sn alloys were analyzed by using X-ray powder diffractometer (X'Pert pro panalytical MRD) at the Ain Sham University, Egypt, and equipped with a CuKα target of (λ=1.54056Å) radiation and a scanning rate of 2^o (2θ)/min. The Rietveld refinement of the XRD peaks was analyzed through (FullProff Suit program 2.05). GFourier program (FullProff package) was used for the calculation and visualization of electron density within the unit cell. Average crystallite size was calculated by Scherrer's formula considering the position and broadening of the most intense diffraction peak in XRD spectra, beside using Williamson-Hall plot for calculation of the particle size and microstrain. The microstructure of the rapidly solidified Al-Sn alloys were observed by scanning electron microscopy (SEM /Hitachi S-4800) at the (Central Metallurgical Research Institute - Helwan- Egypt), utilizes an electron beam accelerated at 500 V to 30 kV, and features a maximum resolution of 1 nm. Maximum magnification is 800,000X. To observe SEM, the alloy sample surface was polished with the silicon carbide abrasive paper, followed by ultrasonic treatment in ethanol for 2 min to remove the oxide layer. TG/DTA 6300 system (Cairo university, Egypt) was used to characterize our samples, the samples exposed to temperatures up to 350 ^oC, with the temperature rise rate up to 20°C/min. The Electrical properties and Temperature dependence of resistivity had been performed for all prepared alloys using an RLC bridge (model: GRUNDIG programmable automatic RLC Meter) with a resistance measurement range (1 mΩ – 99.9 MΩ). For H_2 generation test a water displacement method was used to calculate the volume of the generated hydrogen for the Al-Sn melt spun alloys.

3. Hydrogen generation test

Rapidly solidified Al_{100-x}-Sn_x alloy X= (0, 25, 55, 75 all in wt.%) was prepared using melt spinning technique at 800 ^oC. For the hydrogen generation tests, the prepared alloys were attached using epoxy resin and polished. The area of the specimen exposed to the environment was 2 cm^2, The fixation of the sample was illustrated in fig.1. The hydrogen generation tests were performed in a 2 M NaOH solution at (100 to 110°C) for the Al-Sn melt spun alloys. This is because fast hydrogen generation from the hydrolysis of the Al alloy in bulk form in strong alkaline water. In a weak alkaline medium, the exclusion of passive films like Al_2O_3 and $Al(OH)_3$ is not possible [19]. The temperature for the reaction was maintained by a digital thermocouple. The volume of producing hydrogen gas was measured using the water displacement method as cited elsewhere [20]. In this specific experiment, a 1000 ml measuring cylinder filled with water was employed in a plate partially filled with water and a silicon tube connected to the reaction flask was inserted inside the cylinder, as shown in Fig.2. As the H_2 flow starts, the gas through the silicon tube comes in the cylinder. The H_2 gas started to be generated at the top of the cylinder, and displaces water over its pressure.

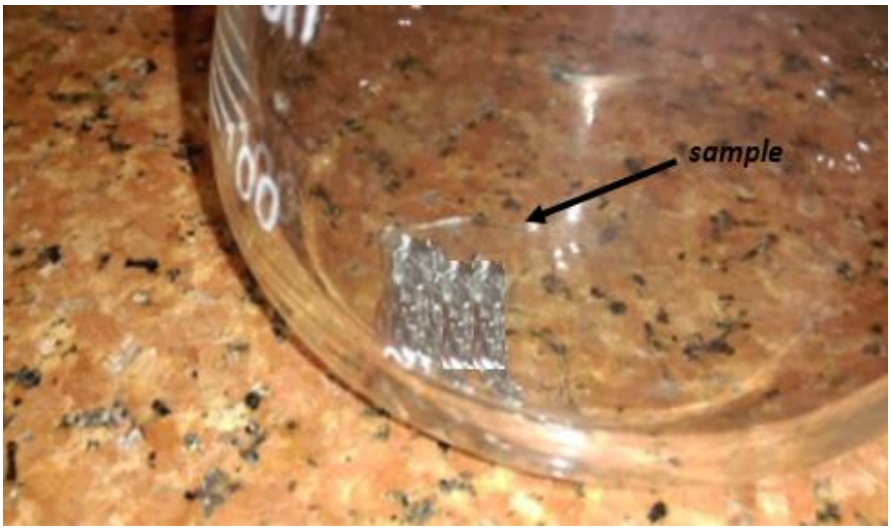

Fig.1. The fixation of sample with epoxy resin.

ISSN 2347-3487
Volume 13 Number 6
Journal of Advances in Physics

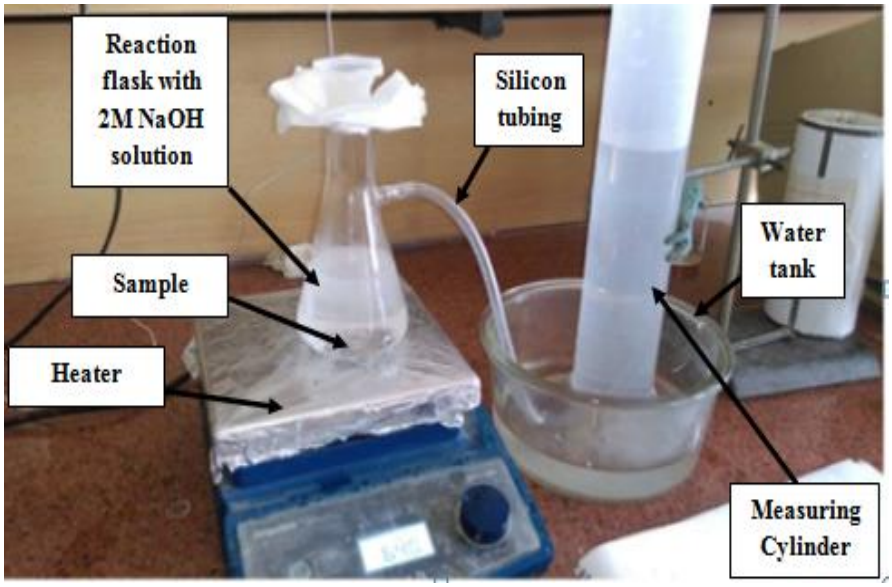

Fig.2 . Experimental set-up for the hydrogen measurement

4. Results and discussion

4.1 X-ray Diffraction Measurement for The Al-Sn alloy System

X-ray diffraction analysis by computer search matching for the pure Al, Al-45% Sn, Al-75% Sn, and Al-25% Sn samples showed that sample consisted of two phases of pure Al and β-Sn. It is observed that the peak corresponding to the planes (1 1 1), (2 0 0), (2 2 0) and (3 1 1) confirming the phase formation of pure Al with a well defined face centered cubic structure (FCC) of space group (F m -3 m) and coinciding with the (ICCD:03-065-2869).And the peak corresponding to the planes (2 1 1), (1 0 1), (3 0 1), (2 0 2), (3 2 1) and (2 1 1) confirming the phase formation of pure β-Sn with a well defined tetragonal structure of space group (I 41/a m d) and coinciding with the (ICCD: 03-065-0296). Fig.3 represents the X-ray diffraction patterns of pure Al, $Al_{25}Sn_{75}$, $Al_{75}Sn_{25}$, and $Al_{45}Sn_{55}$samples.

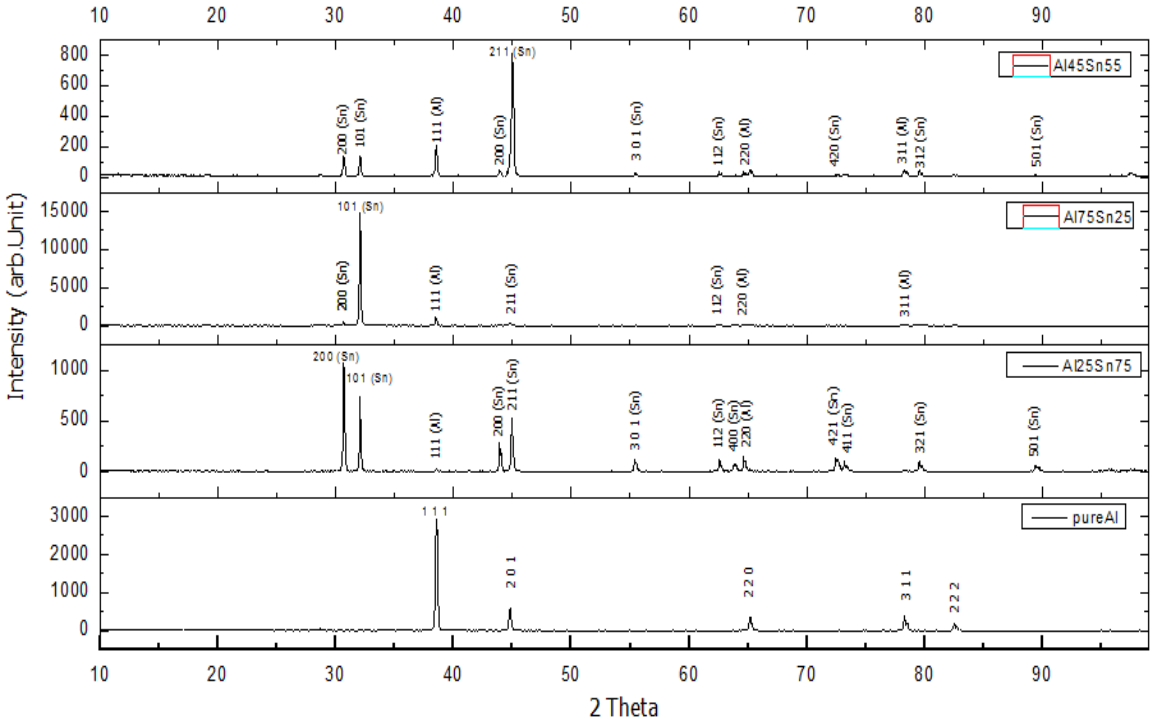

Fig.3. XRD patterns for pure Al, $Al_{25}Sn_{75}$, $Al_{75}Sn_{25}$, and $Al_{45}Sn_{55}$alloys,prepared by melt spinning technique.

ISSN 2347-3487
Volume 13 Number 6
Journal of Advances in Physics

4.1.1 Refinement Results and Discussion

In the Rietveld analysis of X-ray diffraction data of the four alloy systems (Pure-Al, $Al_{25}Sn_{75}$, $Al_{75}Sn_{25}$, and $Al_{45}Sn_{55}$), we employed the software (FULLPROF) using the Rietveld method. It is designed to refine simultaneously both the structural (lattice cell constants, atomic positions and occupancies) and microstructural parameters (crystallite size and lattice micro strain). The shape of the peaks in the experimental diffraction patterns was well described by an asymmetric pseudo-Voigt (PV) function. To simulate the theoretical x-ray diffraction patterns of the prepared alloy systems the following considerations for the different phases we made:

1- Identification of the phases by computer search-match to compare the actual experimental patterns with the International Centre for Diffraction Data (ICCD) database of known materials.

2- Index the diffraction pattern to determine the crystal system, unit cell dimensions and space group.

i. The pure aluminium Al with face centered cubic structure (FCC), space groups: Fm-3m (225).

ii. β-sn sample has Tetragonal structure, space group I41/amd (141).

In each refinement, a total of more than twenty parameters were refined: zero shift, scale factor, background coefficients, three lattice constants, asymmetry factor, and parameter for the full width at half maximum.

The Rietveld plots of the refinements for pure-Al, $Al_{25}Sn_{75}$, $Al_{75}Sn_{25}$, and $Al_{45}Sn_{55}$ prepared alloys are given in fig.4 to Fig.7. In this figure the observed intensity data, y, are plotted in the upper field as points. The calculated patterns are shown in the same field as a solid line curve. The difference between calculated and observed patterns is shown in the lower field. The short vertical bar in the middle field indicates the positions of possible Bragg reflections.

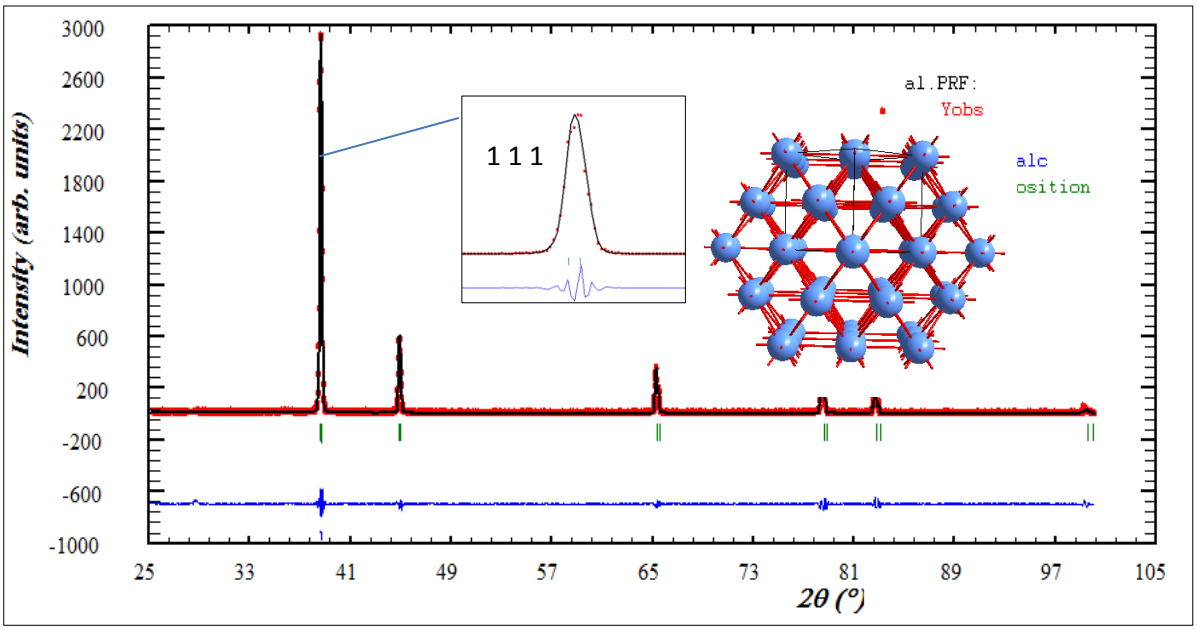

Fig.4. The profile fitting for pure-Al alloy prepared by melting spinning technique using (FULLPROF) software.

ISSN 2347-3487
Volume 13 Number 6
Journal of Advances in Physics

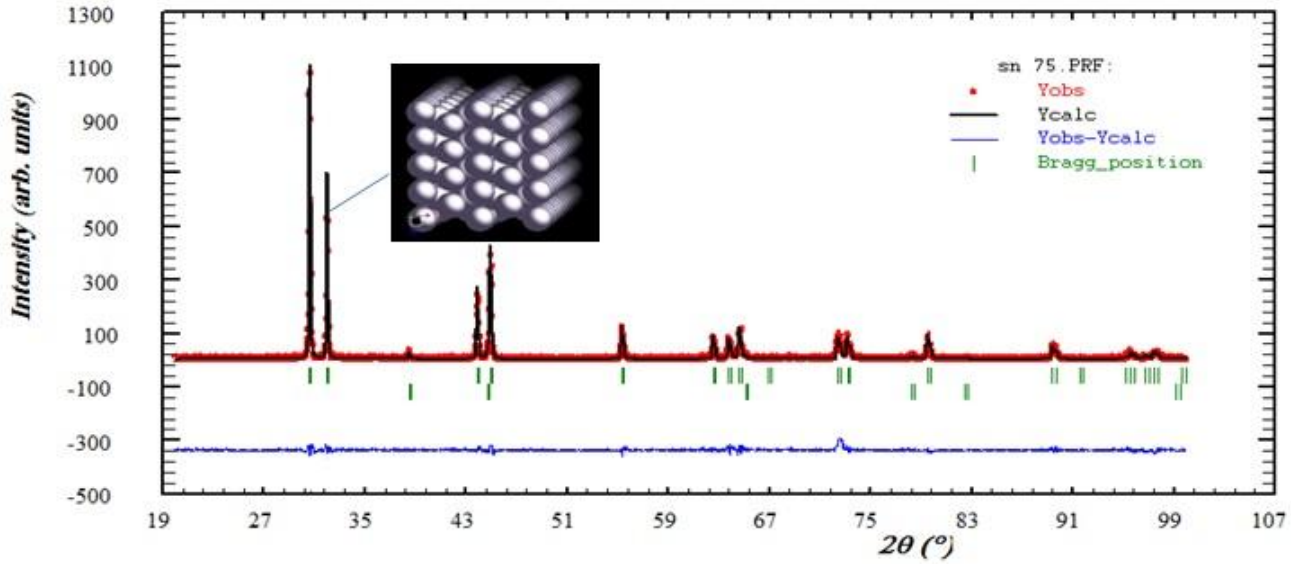

Fig.5. The profile fitting for $Al_{25}Sn_{75}$ alloy prepared by melting spinning technique using (FULLPROF) software.

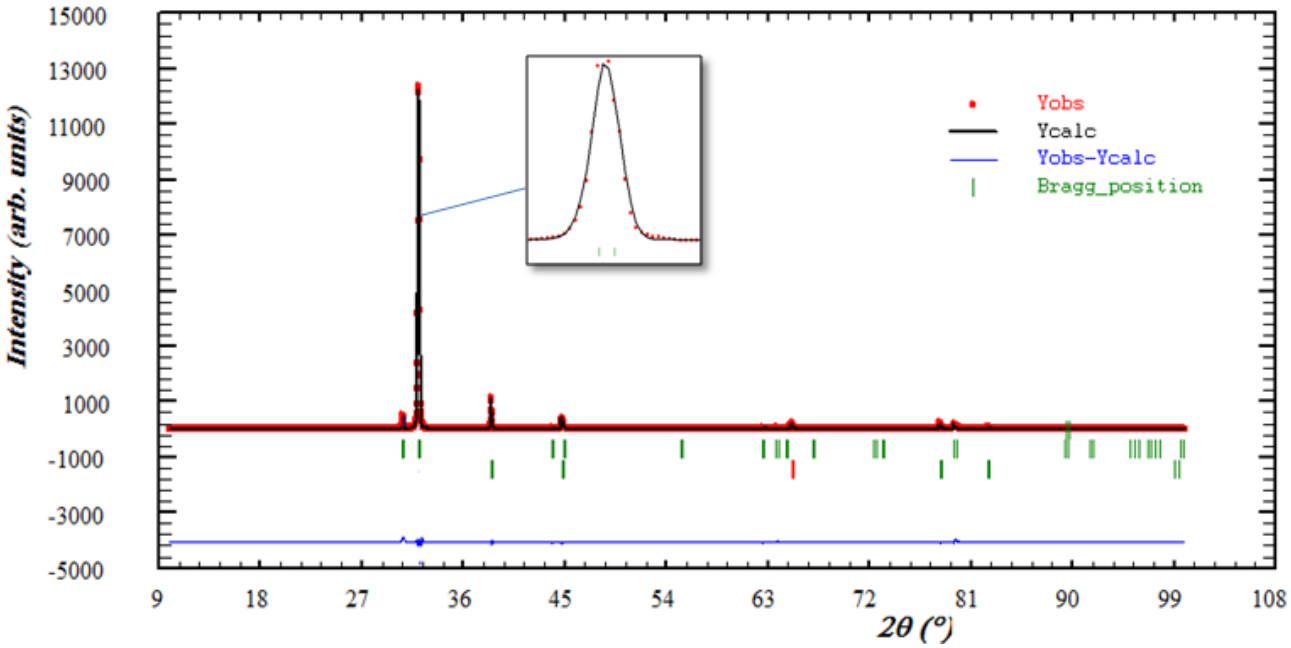

Fig.6. The profile fitting for Al75Sn25 alloy prepared by melting spinning technique using (FULLPROF) software

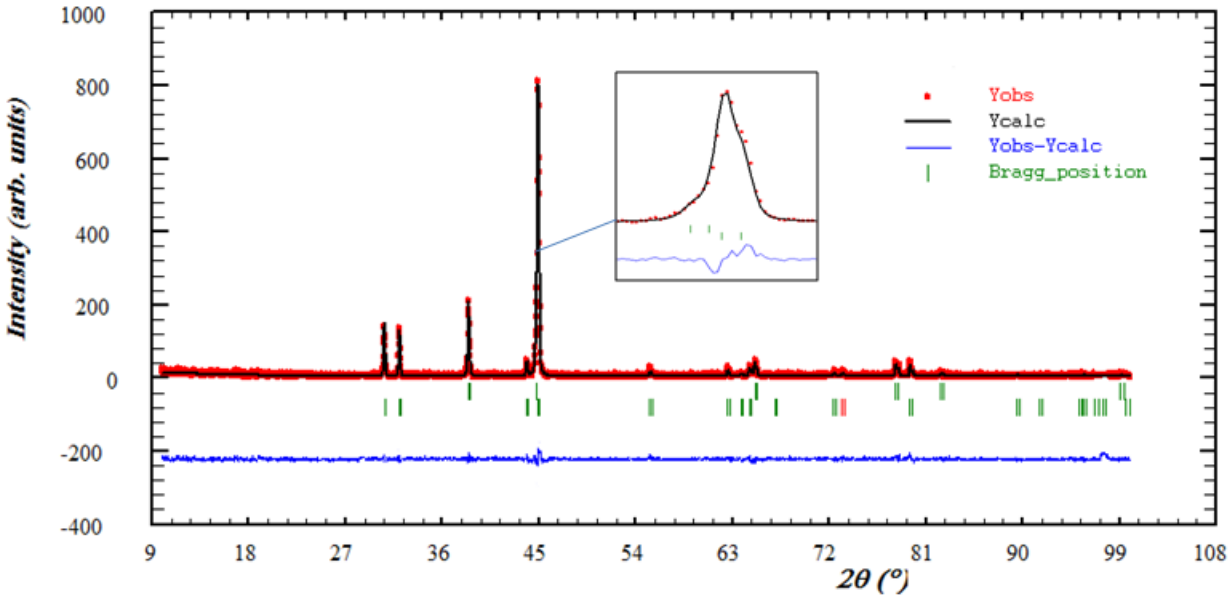

Fig.7. The profile fitting for $Al_{45}Sn_{55}$ alloy prepared by melting spinning technique using (FULLPROF) software

The fitting parameters for the investigated samples, prepared by melt spinning technique are displayed in table (1). The goodness of profile fit (GoF) value of all samples indicates that the profile was fitted successfully.

Table (1): The fitting parameters for prepared alloys.

Composition	GoF	Bragg R-factor	RF-Factor
Pure-Al	1.38	4.833	6.221
Al25Sn75	1.19	Al 7.057	Al 7.55
		β-Sn 8.714	β-Sn 6.59
Al75Sn25	1.12	Al 6.054	Al 7.120
		β-Sn 4.410	β-Sn 4.714
Al45Sn55	1.10	Al 9.082	Al 8.880
		β-Sn 8.060	β-Sn 7.860

4.1.2 Electron density Maps, and calculations

GFourier program was used for the calculation and visualization of electron density within the unit cell. The visualization is very useful in identifying the atomic positions of constituent elements within the unit cell for known or unknown crystals, i.e. denser the electron density contours indicate the position of a heavier element among the constituent elements in the unit cell. In the world of crystallography, You may wonder about this use of the Fourier transform. The scattering density ρ(x,y,z) is usually calculated according to the equation:

$$\rho(x,y,z) = \frac{1}{V}\sum_{hkl} |F_{(hkl)}| e^{\{-2\pi i\,(hx+ky+lz-\alpha_{hkl})\}}$$

Where,ρ(x,y,z) is the electron density at a point x,y,z in a unit cell of volume V, F(hkl) is the structure factor amplitude and α_{hkl} is the phase angle of each Bragg reflection (h,k,l).

Two-dimensional maps are typically drawn with contours (and sometimes colour) to indicate different density levels, while three-dimensional maps employ a chicken-wire style mesh representing a single level. (The latter works very well in protein crystallography, where 99% of the atoms (excluding H) scatter near identically.) Some typical 2-dimensional maps of the plane z = 0 for Al and Sn phases are calculated using X-ray structure factors are shown below in Figures 8 and 9.

ISSN 2347-3487
Volume 13 Number 6
Journal of Advances in Physics

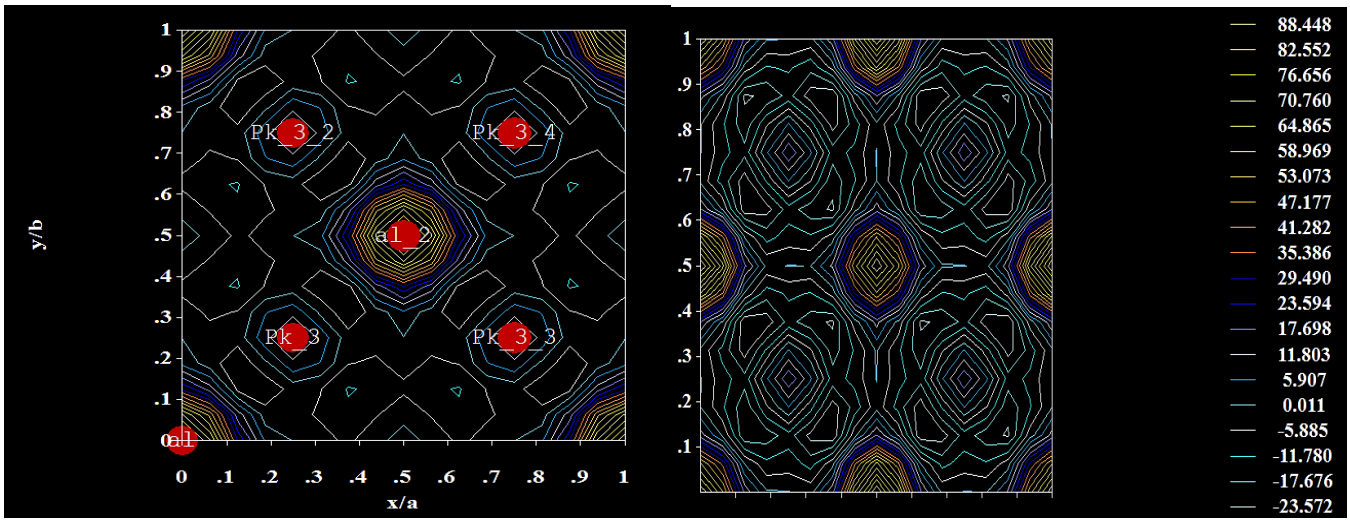

Fig.8. 2D Electronic density map of individual atoms in the unit cell of pure-Al alloy at z=0.

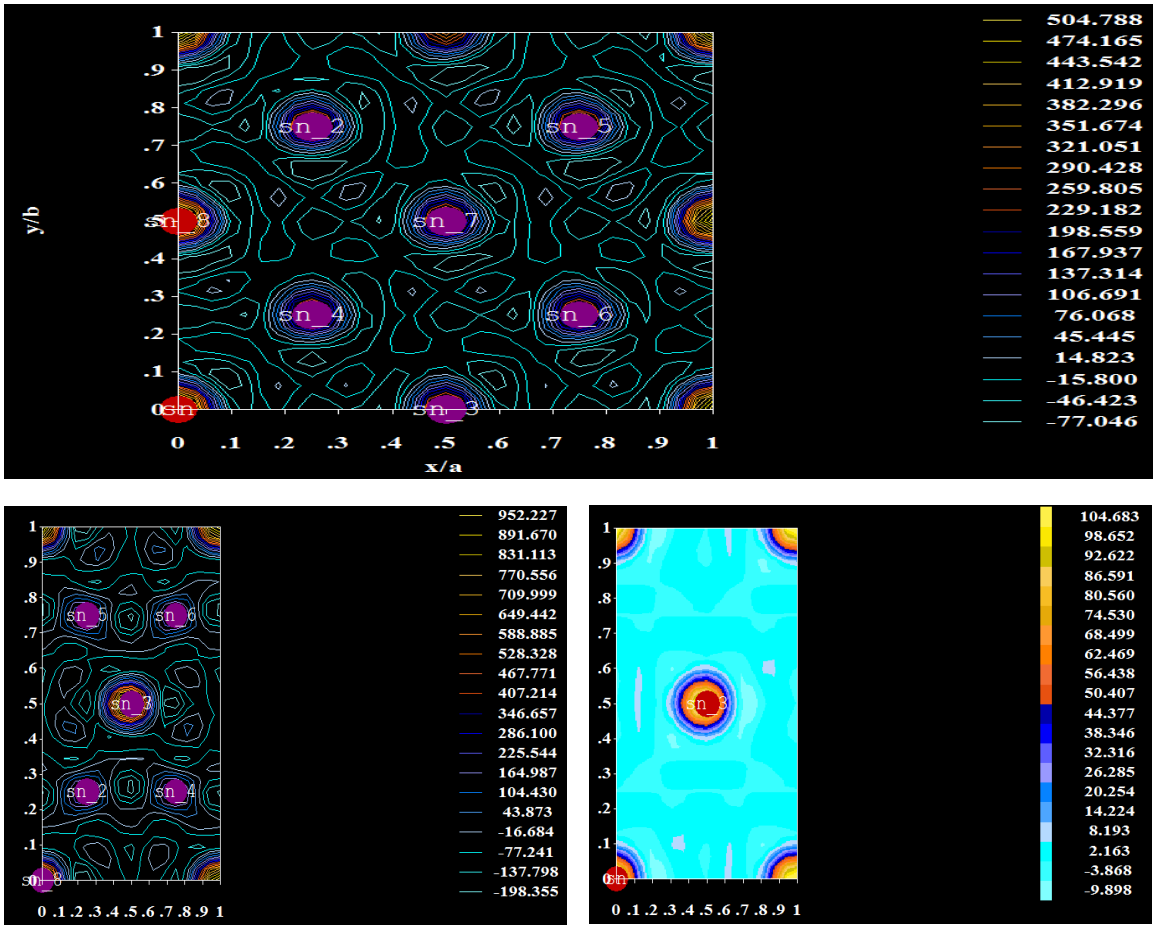

Fig.(9.a). 2D Electronic density map of individual atoms in the unit cell of β-Tin.

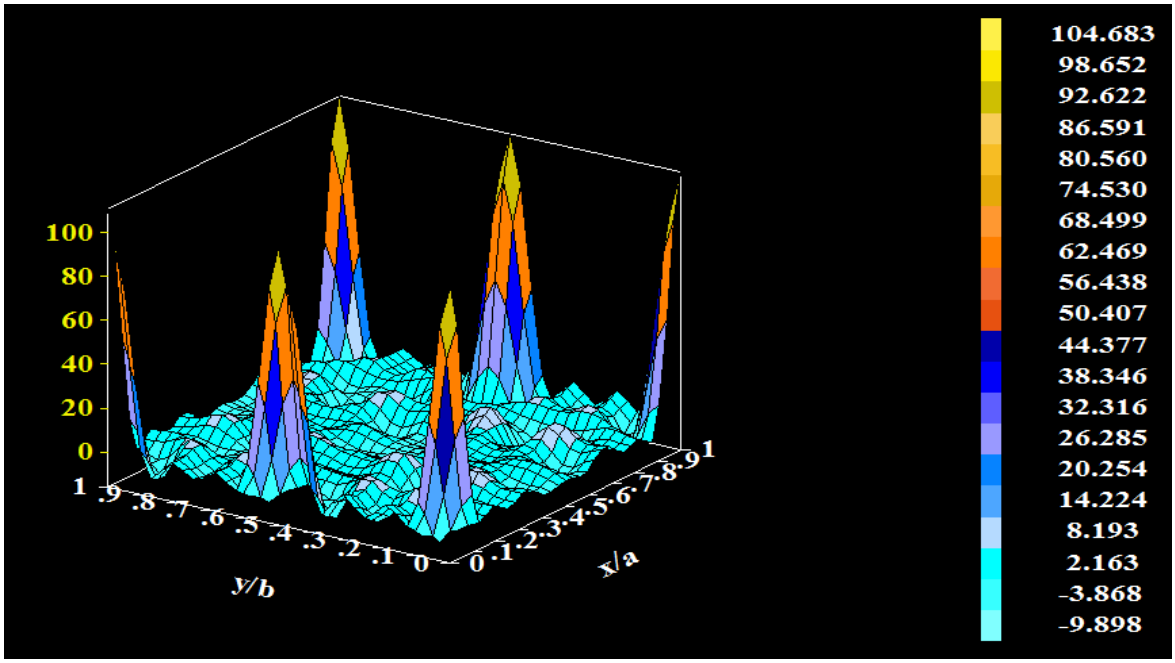

Fig. (9.b) 3D-contour map of Electronic density for β-Tin phase.

The zero level density contour is shown in black, while the colors red through to violet-brown region indicates increasing levels of electron density around Al and Sn phases.

4.2 Thermal analysis of Al-Sn Alloys

Differential Thermal Analysis (DTA) is performed for as quenched alloys in the temperature range from 300 to 1000 K at a heating rate of 10 K min^{-1} by a DTG-60H. Fig. (10.a) shows the DTA scan in the temperature range for rapidly solidified pure Al alloys. It shows that, no phase transformation has been observed before melting, which occurred at 931.2 K compared with 933.47 K for conventional Al. The enthalpy and entropy of fusion is estimated from the endothermic peak area and the results are; the value of ΔH^{fc} for pure Al rapidly solidified was found to be 7.07 $kJ.kg^{-1}$ compared with 10.71 $kJ.kg^{-1}$ for conventional Al. i.e. the enthalpy of fusion is decreased by 3.64 $kJ.kg^{-1}$.

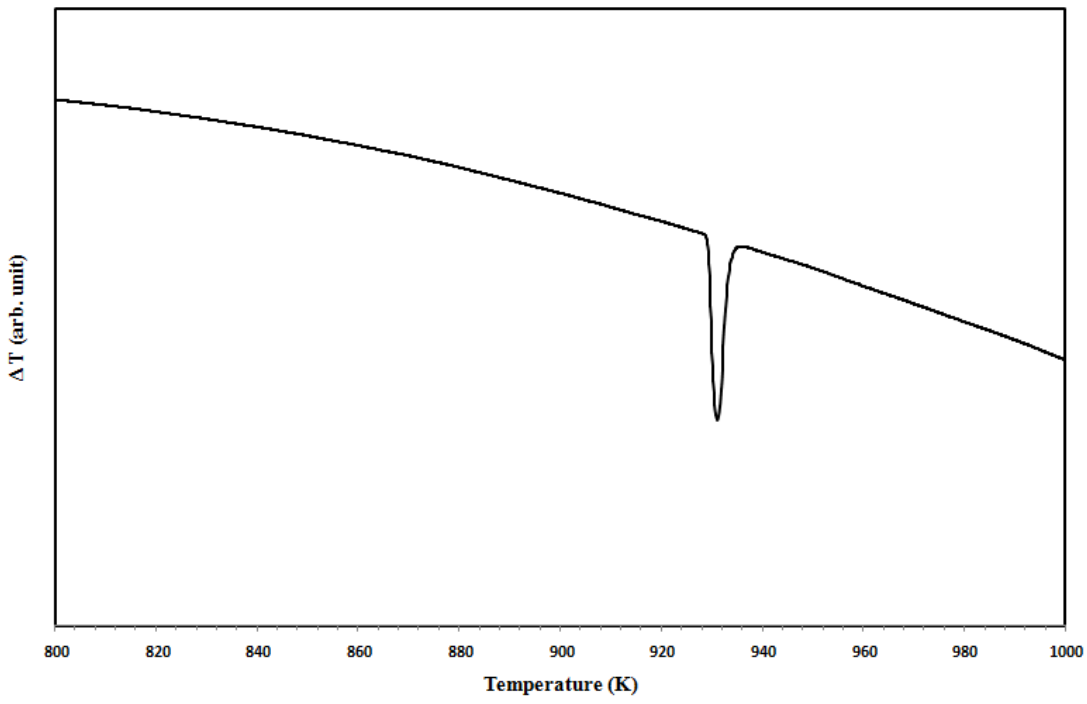

Fig.(10.a) The differential Thermal Analysis (DTA) of as-quenched melt spun pure Al.

The melting temperature (T_m^{cc}) for pure Al produced by CC is 933.47 K, the enthalpy of fusion is (ΔH^{cc}) 10.71 kJ.kg^{-1} and the entropy of fusion ΔS^{cc} fusion = ΔH^{cc} fusion/ T_m^{cc} fusion= 11.47 J.kg^{-1}.K^{-1}. For pure Al produced by RS, (T_m^{RS}) is found to be 931.2.1 K, ΔH^{RS}= 7.07 kJ.kg^{-1} and ΔS^{RS} fusion = ΔH^{RS} fusion/ T_m^{RS} fusion= 7.57 J.kg^{-1}.K^{-1}. Now, let us calculate the change in enthalpy (ΔH_v) and entropy (ΔS_v) due to the presence of vacancies. As $\Delta H_f^{CC} = H_l^{CC} - H_s^{CC}$ and $\Delta H_f^{RS} = H_l^{RS}-H_s^{RS}$, hence, $\Delta H_f^{CC} - \Delta H_f^{RS} = H_s^{RS} - H_s^{CC} + H_l^{CC} - H_l^{RS}$, by assuming that in the liquid state and at the same temperature, $H_l^{CC} = H_l^{RS}$, therefore, $\Delta H_f^{CC} - \Delta H_f^{RS} = H_s^{RS}-H_s^{CC}$, from which we obtain $H_s^{RS} - H_s^{CC}$ = 10.71– 7.07 = 3.64 kJ.kg^{-1}. This means that the enthalpy of RS pure Al is increased. Assuming that the formation of vacancies is the most important effect of rapid solidification in this case, the enthalpy increase due to the presence of vacancies is estimated to be ΔH_v= 3.64 kJ.kg^{-1}. Similarly, we can calculate the increase in entropy due to the formation of vacancies: $\Delta S_f^{CC} - \Delta S_f^{RS} = S_s^{RS}-S_s^{cc}$, from which $S_s^{RS}-S_s^{cc}$ = 11.47 – 7.57 = 3.9 J.kg^{-1}.K^{-1}. The change in the free energy is given by$\Delta G_v = \Delta H_v - T\Delta S_v$, where T is the temperature just before melting (929.1 K). Substituting for ΔH_v and ΔS_v then we can obtain ΔG_v = 7029.83 J.kg^{-1}.

Fig. (10.b) shows the DTA curve for $Al_{75}Sn_{25}$, $Al_{25}Sn_{75}$ and $Al_{45}Sn_{55}$ alloys. The details of thermal analysis using DTA for all alloys are summarized in Table (1).

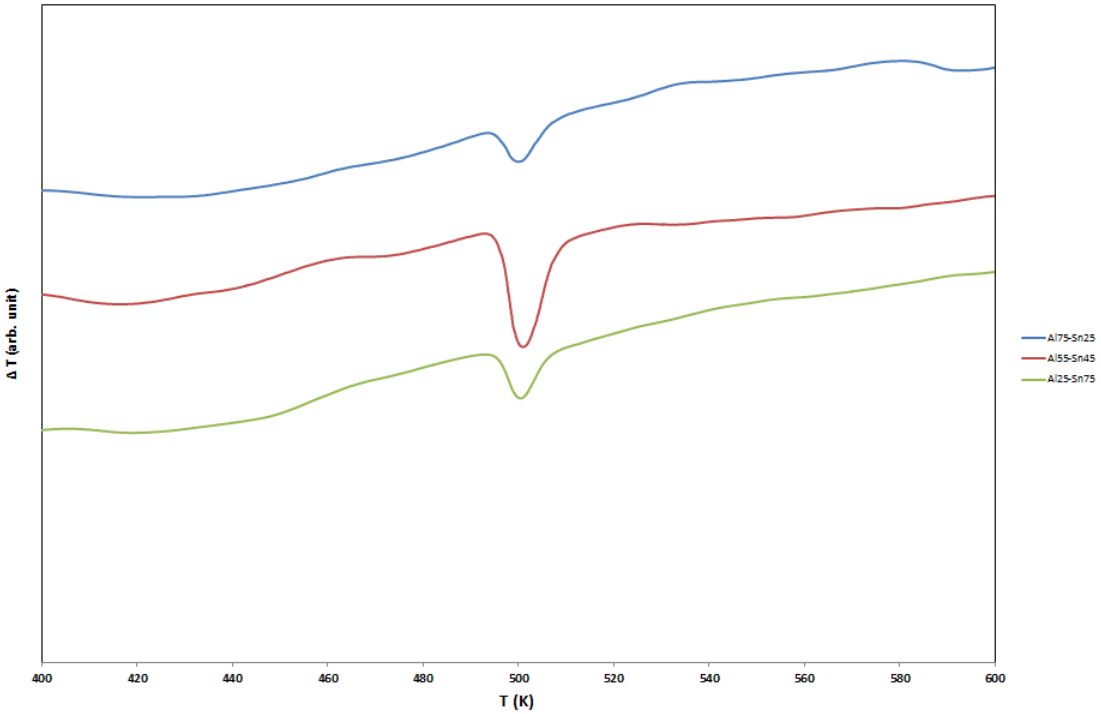

Fig.(10.b) The differential Thermal Analysis (DTA) of as-quenched melt spun $Al_{75}Sn_{25}$, $Al_{25}Sn_{75}$ and $Al_{45}Sn_{55}$alloys.

Table (1): Thermal parameters for the prepared alloys calculated using DTA.

Alloy	T (onset) (K)	T melting (K)	T (offset) (K)	ΔH (KJ/Kg)	ΔS (J/Kg.K)	ΔG (J/Kg)
Pure Al	929.1	933.47	936.2	7.07	7.573891	7062.93
Al_{25}-Sn_{75}	493.13	499.56	511.33	15.84	31.707903	15824.16
Al_{55}-Sn_{45}	495.17	500.95	519.44	44.11	88.0527	44065.89
Al_{75}-Sn_{25}	489.93	499.93	512.23	19.45	38.905447	19430.55

4.3 Hydrogen generation using the corrosion of Al-Sn alloys in an alkaline solution

Rapidly solidified Al_{100-x}-Sn_x alloy, X= (0, 25, 55, 75 all in wt.%) were immersed in 2 M NaOH solution at 95 °C, and the volume of generating hydrogen of the solution by immersing the alloys was recorded, as shown in Fig.11.

The volume of hydrogen generation varied from 210 ml for pure Al to 531 ml for $Al_{45}Sn_{55}$ at 3.5 min. For the *$Al_{45}Sn_{55}$* alloy, the amount of generating hydrogen was the highest at 531 ml among all the measurements at 95 °C. The as-quenched melt spun 55 wt % Sn alloy showed saturation in the hydrogen generation rate after 3.23 min. While the 25 wt% and 75 wt% Sn alloys exhibited a saturation of hydrogen generation at 320 and 235 ml, respectively. The higher hydrogen generation for the melt spun alloys might be owing to the good distribution of Sn along the Al grains at the surface and the resulting shorter path of electron between Sn and Al in galvanic corrosion.

In our work, the most important effect of the addition of Sn was the shortening of delay time, so that the reaction process started instantly after the sample came in direct contact with alkaline solution. This is owing to the creation of galvanic cells between the Al grain and close Sn phase. The existence of the Tin phase in grain boundaries can accelerate the corrosion of Al grains by galvanic effect and the consequential hydrogen production.

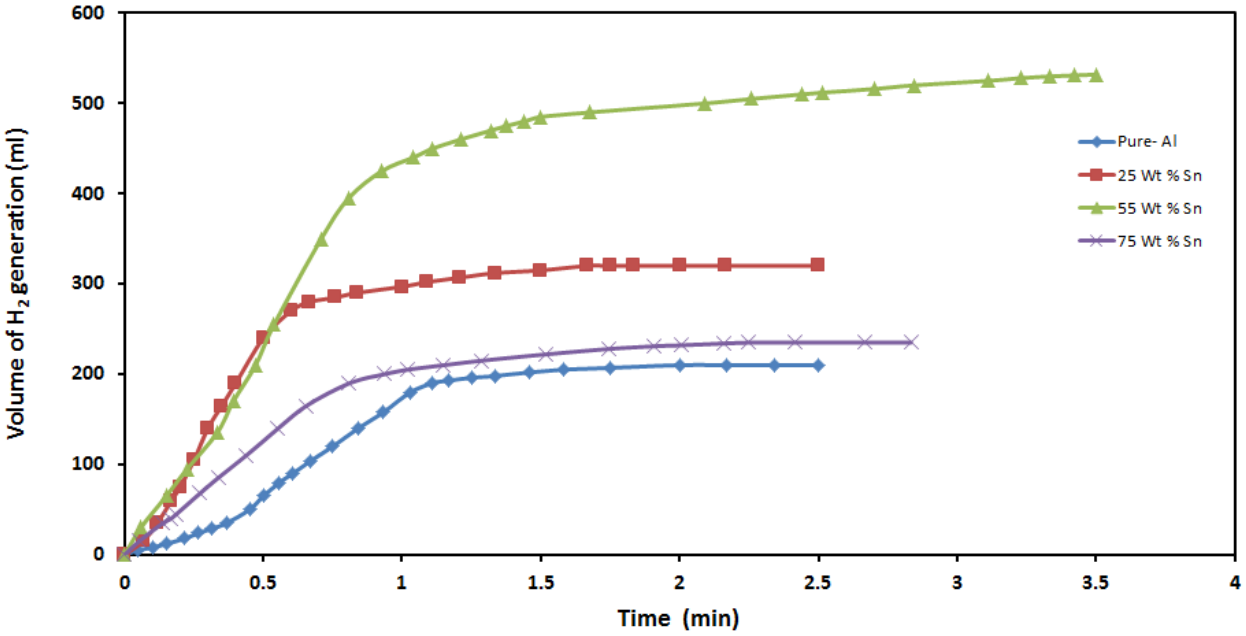

Fig.11. The Volume of hydrogen generation from 2 M NaOH solution of as-quenched melt spun Al-Sn alloys.

Also, the reaction kinetics increased with increasing the solution temperature. The delay time declined from tens of minutes to a few minutes with increasing Sn to Al weight ratio. The lesser delay time or shorter reaction duration was observed more strikingly in the higher Sn containing alloy. A simple mechanism was recommended for galvanic corrosion and H_2 production in prepared Al-Sn alloys, as shown in Fig.12.

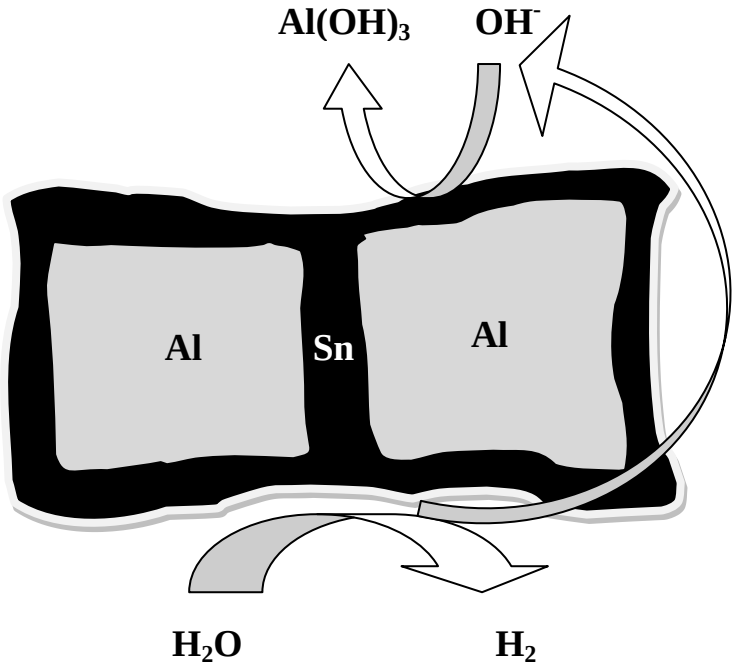

Fig.12. Schematic illustration of for corrosion and H_2 generation mechanism in Al-Sn alloys.

Galvanic cells were formed between the Al grain and surrounding Tin, where the Al grain represents an anode and the Sn phase acts as a cathode. Al is oxidized to form an Al^{3+} ion and hydrogen is grown-up over the reduction of water on the surface of the Tin phase. A latest research [21] described that beta Sn phase can act as cathodic centers

through the corrosion development in the chemical etching of Al-Sn alloys because Sn is a better catalyst for H_2 progression than Al [22]. Rendering to earlier studies [23], the metallic Sn particles covering the Al particles can act as cathodic centers to generate H_2 via reaction (2), while Al acts as an anodic center for oxidation through reaction (1) by creating a galvanic cell. Reaction (3) indicates the complete reaction:

$$\frac{1}{3}\,\mathbf{Al} \rightarrow \frac{1}{3}\,\mathbf{Al^{+3}} + \mathbf{e^-} \qquad \textbf{(1)}$$

$$\mathbf{H_2O} + e^- \rightarrow \frac{1}{2}\,\mathbf{H_2} + \mathbf{OH^-} \qquad \textbf{(2)}$$

$$\frac{1}{3}\,\mathbf{Al} + \mathbf{H_2O} \rightarrow \frac{1}{3}\,\mathbf{Al(OH)_3} + \frac{1}{2}\,\mathbf{H_2} \qquad \textbf{(3)}$$

This galvanic corrosion can make the hydrogen evolution on the surface of the Al-Sn alloys become larger than that of pure Al.

4.4. Microstructure of Al-Sn Alloys

The microstructure of the rapidly solidified Al-Sn alloys were examined. Figures(13.a) to (13.d) shows the microstructural analysis of the rapidly solidified Al-Sn alloys prepared by melting spinning technique, the grain distributions and average grain size were calculated using an SPM data visualization and analysis tool (Gwyddion 2.32), see table (2) . In our work we mainly focused on nonuniform distribution of Sn particles through the spinning process in a molten Al-Sn alloy. The Al-Sn alloys exhibited a network structure of a β-Sn second phase surrounding the Al grains.The Al phase nucleated and grew from the existing Al matrix, and left the Sn phase along the boundaries of the Al grains. In the SEM images, the white part represents the Sn phase, and the gray black part is the Al phase, with an increasing Sn content, the brighter Sn phase in grain boundaries became denser. Evidently, the Sn phase enclosed the granular Al matrix. In addition, the Al grain size decreased with an increasing Sn content.

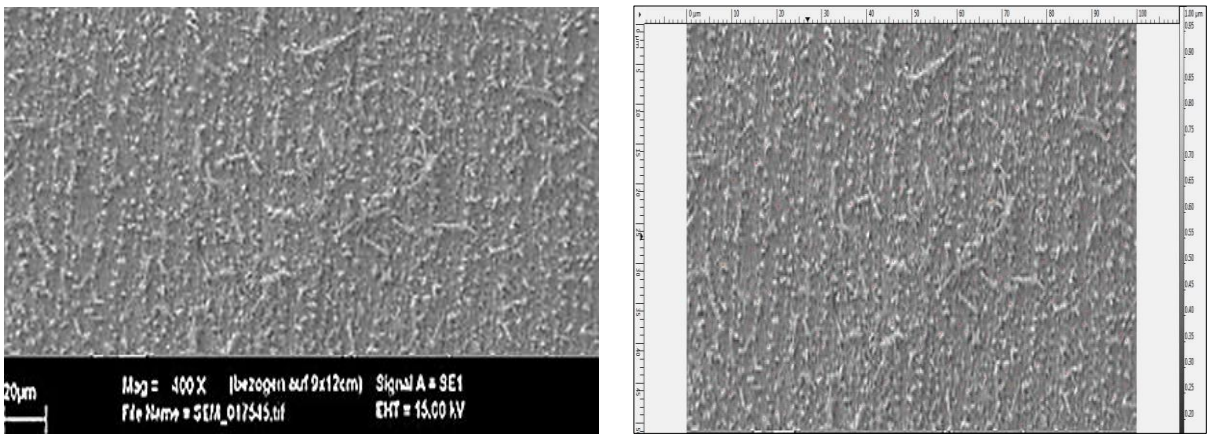

Figure (13.a): SEM images of the rapidly solidified pure Al.

ISSN 2347-3487
Volume 13 Number 6
Journal of Advances in Physics

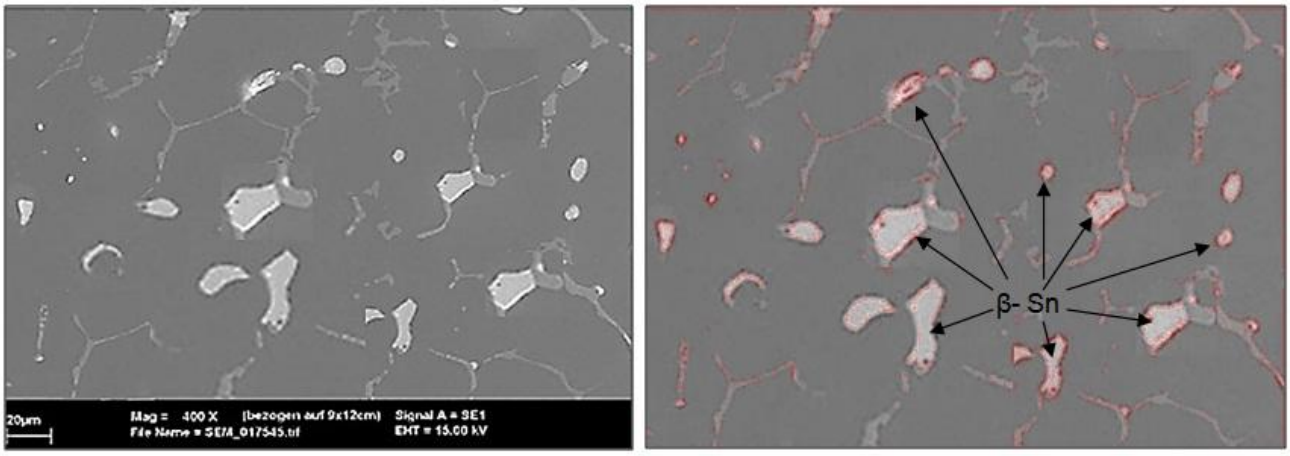

Fig. (13.b): SEM images of the rapidly solidified $Al_{75}Sn_{25}$alloy.

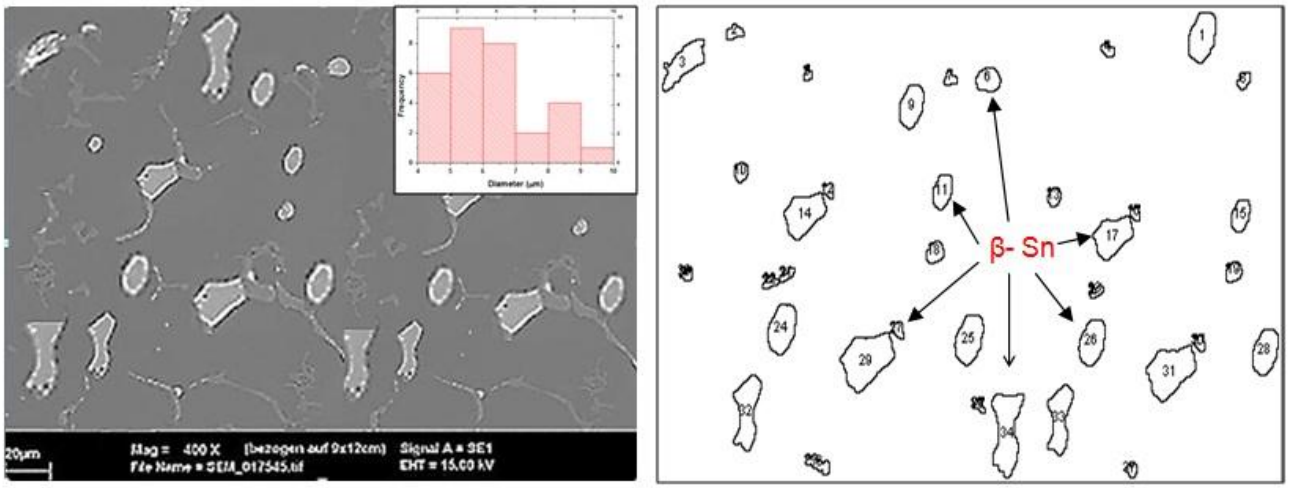

Fig. (13.c): Microstructural analysis of the rapidly solidified $Al_{25}Sn_{75}$alloy.

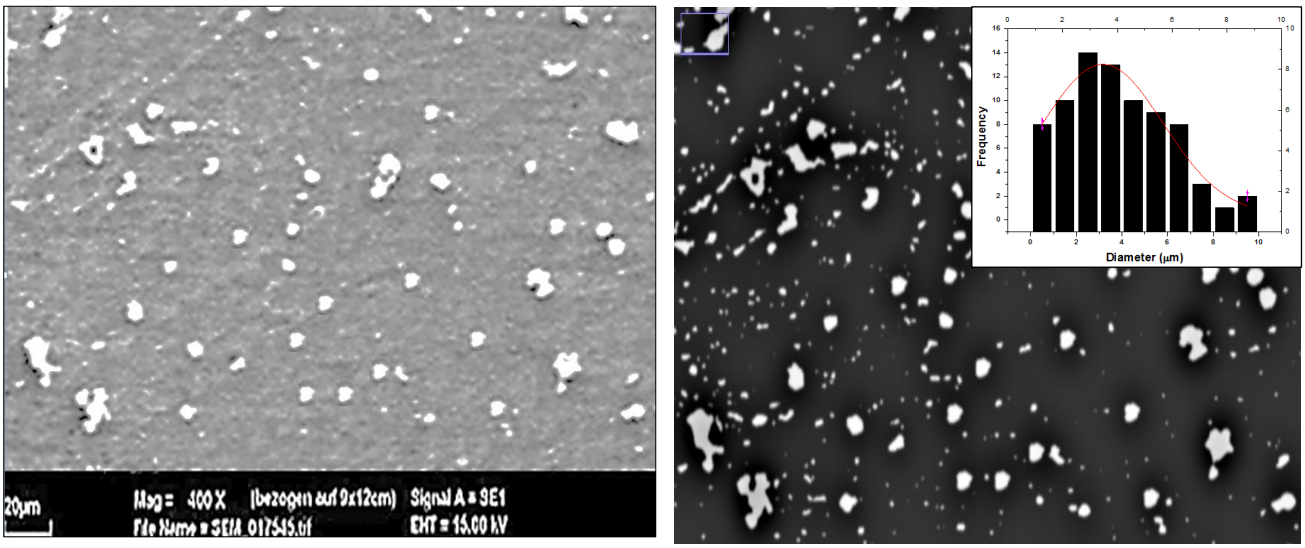

Fig. (13.d): Microstructural analysis of the rapidly solidified $Al_{45}Sn_{55}$alloy.

Table (2): Microstractural parameters for the prepared alloys calculated using an SPM data visualization and analysis tool (Gwyddion 2.32).

Alloy	Number of grains	Total projected area (μm^2)	Mean grain area (m^2)	Mean grain size (nm)	Total grain volume (μm^3)	Total projected boundary length (µm)
Pure Al	360	20.6	$57 *10^{-15}$	238	13.3	247
Al25-Sn75	112	7.3	$65* 10^{-15}$	242	4.2	88
Al55-Sn45	1096	88	$80*10^{-15}$	246	65	1.12 mm
Al75-Sn25	164	8.1	$49*10^{-15}$	204	6	112

Conclusion

Rapidly solidified Al_{100-x}-Sn_x alloy X= (0, 25, 55, 75 all in wt.%) was prepared using melt spinning technique at 800 °C. the structure and microstructural analysis were characterized usind X-ray diffraction and rietveld analysis, which confirms the presense of two pases of pure Al with a well defined face centered cubic structure (FCC) of space group (F m -3 m) and β-Sn with a well defined tetragonal structure of space group (I 41/a m d).

From the Differential thermal analysis it is found that all the produce alloys are stable. Melting temperature reduced from 933.47 K for Al pure to 500.95 K in $Al_{45}Sn_{55}$.

Rapidly solidified Al_{100-x}-Sn_x alloy, X= (0, 25, 55, 75 all in wt.%) were immersed in 2 M NaOH solution at 95 °C. The best volume of hydrogen generation which is (531 ml) is for $Al_{55}Sn_{45}$ alloy due to the good distribution of Sn along the Al grains at the surface and the resulting shorter path of electron between Sn and Al in galvanic corrosion.

The Al-Sn alloys exhibited a network structure of a β-Sn second phase surrounding the Al grains, through SEM. The Al phase nucleated and grew from the existing Al matrix, and left the Sn phase along the boundaries of the Al grains. It is found that the greatest numbers of grains is for $Al_{55}Sn_{45}$ alloy (1096).

References

1. W. C. Lattin and V. P. Utgikar, *Int. J. Hydrogen Energ*. 32, 3230 (2007).

2. M. S. Zou, R. J. Yang, X. Y. Guo, H. T. Huang, J. Y. He, and P. Zhang, *Int. J. Hydrogen Energ*. 36, 6478 (2011).

3. S. H. Yu, J. Y. Uan, and T. L. Hsu, *Int. J. Hydrogen Energ.*37, 3033 (2012).

4. X. Ma and M. R. Zachariah, *Int. J. Hydrogen Energ*. 35, 2268 (2010).

5. J. Macanás, L. Soler, A. María Candela, M. Muñoz, and J. Casado, *Energy*, 36, 2493 (2011).

6. K. Wegner, H. C. Ly, R. J. Weiss, S. E. Pratsinis, and A. Steinfeld, *Int. J. Hydrogen Energ.* 31, 55 (2006).

7. I. Vishnevetsky and M. Epstein, *Int. J. Hydrogen Energ*. 32, 2791 (2007).

8. C. Y. Cho, K. H. Wang, and J. Y. Uan, *Mater. Trans.* 46, 2704 (2005).

9. M. H. Grosjean, M. Zidoune, L. Roue, and J. Y. Huot, *Int. J. Hydrogen Energ.* 31, 109 (2006).

10. M. H. Grosjean and L. Roue, *J. Alloy. Compd*. 416, 296 (2006).

11. J. Y. Uan, C. Y. Cho, and K. T. Liu, *Int. J. Hydrogen Energ*. 32, 2337 (2007).

12. S. S. Martınez, W. L. Benıtes, A. A. A. Gallegos, and P. J. Sebastian, *Sol. Energ. Mat. Sol. C*. 88, 237 (2005).

13. O. V. Kravchenko, K. N. Semenenko, B. M. Bulychev, and K. B. Kalmykov*, J. Alloy. Compd*. 397, 58 (2005).

14. M. J. Baniamerian and S. E. Moradi, *J. Alloy. Compd*. 509, 6307 (2011).

15. K. S. Eom, E. A. Cho, and H. S. Kwon, *Int. J. Hydrogen Energ*. 36, 12338 (2011).

16. M. J. Kim, K. S. Eom, J. Y. Kwon, E. A. Cho, and H. S. Kwon, *J. Power Sources*, 217, 345 (2012).

17. A. Norbert and H. Sven, *Energy*, 31, 1395, (2006).

18. H. S. Yoo, H. Y. Ryu, S. S. Cho, M. H. Han, K. S. Bae, and H. H. Lee, *Int. J. Hydrogen Energ*. 36, 15111 (2011).

19. K. S. Eom, M. J. Kim, S. K. Oh, E. A. Cho, and H. S. Kwon, *Int. J. Hydrogen Energ*. 36, 11825, (2011).

20. J. C. Ingersoll, N. Mani, J. C. Thenmozhiyal, and A. Muthaiah,

J. Power Sources, 173, 450 (2007).

21. M. Nestoridi, D. Pletcher, R. J. K. Wood, S. Wang, R. L. Jones, and K. R. Stokes, J. Power Sources 178, 445 (2008).

22. S. Trasatti, J. Electroanal. Chem. 39, 163 (1972).

23. M. Q. Fan, F. Xu, and L. X. Sun, Int. J. Hydrogen Energy. 32, 2809 (2007).